Positron backscattering from elemental solids

1992 J. Phys.: Condens. Matter 4 10311

(http://iopscience.iop.org/0953-8984/4/50/018)

J. Phys.: Condens. Matter 4 (1992) 10311–10322. Printed in the UK

Positron backscattering from elemental solids

P G Coleman†, L Albrecht†, K O Jensen‡ and A B Walker†

† School of Physics, University of East Anglia, Norwich NR4 7TJ, UK

‡ Department of Physics, University of Essex, Wivenhoe Park, Colchester CO4 3SQ, UK

Received 3 September 1992

Abstract. New measurements and Monte Carlo simulations of the total coefficients η_+ for the backscattering of positrons from elemental solids are reported as a function of atomic number Z between 13 and 82, incident energies E from 1 to 50 keV, and incident angles between 0° and 65°. The measurements and simulations show generally good agreement with each other and with the recent measurements of Massoumi *et al* and Mäkinen *et al* . Both experiment and simulations suggest that the monotonic increase of η_+ with Z seen at high E is not observed for E below 10 keV. Where possible, the new results are compared with earlier measurements of electron coefficients.

1. Introduction

In recent years the need for a reliable description of the interactions of positrons implanted into the subsurface regions of solids has grown with the development of positron implantation spectroscopy as a tool for non-destructive evaluation of layered structures, for the depth profiling of subsurface defects, and for other surface and near-surface investigations [1]. The differences and similarities between electron and positron interactions are also of considerable interest, and an understanding of positron collision processes in solids underpins and strengthens the description of the equivalent electron processes which govern the interpretation of an array of techniques using monoenergetic electrons as probes of solid samples. Our knowledge of these processes can be encapsulated in scattering cross-sections that can be used to find the positron trajectories in a Monte Carlo simulation or to obtain stopping powers and transport cross sections needed for analytic transport theory. To this end Monte Carlo simulations, based on the Penn dielectric function and with no adjustable parameters, have been performed by Jensen and Walker [2–5] and have been very successful in describing recently-measured positron implantation profiles and mean penetration depths [5].

Another stringent test of the integrity of the simulations has been the prediction of the fraction of implanted positrons which are backscattered and leave a sample target. This was the subject of a Monte Carlo study by Valkealahti and Nieminen [6], who in 1984 were not able to compare their results with a comprehensive set of experimental data. Following the early studies of Mills and Wilson [7] the first measurements of total backscattering coefficients η_+ as a function of incident positron energy E from 1 to 30 keV were made by Baker and Coleman [8,9], by measuring the annihilation gamma ray count rate of positrons decaying in the sample (i.e. of those *not* backscattered). They found that η_+ for Al, Cu, Ag and W was a weakly

0953-8984/92/5010311+12$07.50

increasing function of the incident energy E; their results were not, however, in very good agreement with the Valkealahti–Nieminen Monte Carlo calculations [6].

Recently Massoumi *et al* [2,10] have measured doubly-differential backscattering yields for 35 keV positrons incident on a number of solid samples, which showed good agreement with new Monte Carlo simulations described in [2]. This agreement allowed the extrapolation of the experimental results to all angles and subsequent integration to obtain the total coefficients η_+. These new values, although agreeing reasonably well with the simulations, disagreed markedly with the earlier results of Baker and Coleman [8]. This discrepancy prompted our remeasurement of η_+ using a modified version of the UEA magnetic-transport positron beam system [11]. As stated by Baker and Coleman, whereas an electrostatic beam is required for differential measurements, a magnetically-guided system is well suited to the measurements of *total* coefficients as long as backscattered positrons are transported far enough away from the target so that gamma photons from their eventual annihilation are undetectable. Although taking every precaution to meet this last requirement, the experimental geometry employed in the earlier UEA measurements was such that a positron backscattered with high energy through a large angle could have hit the vacuum envelope in front of the sample and annihilated in sight of the Ge gamma ray detector. In this way the measured count rate would be too high and the resulting η_+ values too low, with the underestimation increasing with incident energy E. Part of the reason for this problem was the proximity of the detector to the sample; a second, associated problem was the serious fluctuation of count rate resulting from very small beam movements. Both problems were combatted by modifications to the system, as discussed in section 2.

In sections 4 and 5 new measurements of η_+ are presented and compared with previous positron and electron (η_-) data. Also, new simulation results are given and analytical transport theory used to identify trends in η_+ and η_-.

2. Experimental apparatus

The sample end of the UEA magnetic-transport beam was modified as shown in figure 1. A 72%-efficiency HPGe detector was used, enabling the sample–detector distance to be greatly increased without unacceptable reduction in count rates. Lead shielding was installed around the detector crystal with a 10 cm long, 1 cm wide slit between sample and detector. This essentially allowed only annihilation radiation from the target to be detected, removing the ambiguity discussed in the previous section; count rate fluctuations due to lateral beam movement were also rendered insignificant by virtue of the much increased target–detector separation.

Only counts in the 0.511 MeV photopeak recorded by the Ge detector were used for the current measurements because of the correspondingly high signal:background ratio of approximately 100:1. The background count rate was regularly monitored and subtracted from the total peak counts. The ratio of the total counts in the photopeak to those in the entire Ge pulse height spectrum was found to remain constant throughout the experiment.

For the 'normal incidence' measurements described below the samples were actually tilted by approximately 3° towards the detector, to avoid significant gamma ray absorption/scattering by the samples. (As was confirmed later, η_+ only varies significantly at angles of incidence above about 30°.)

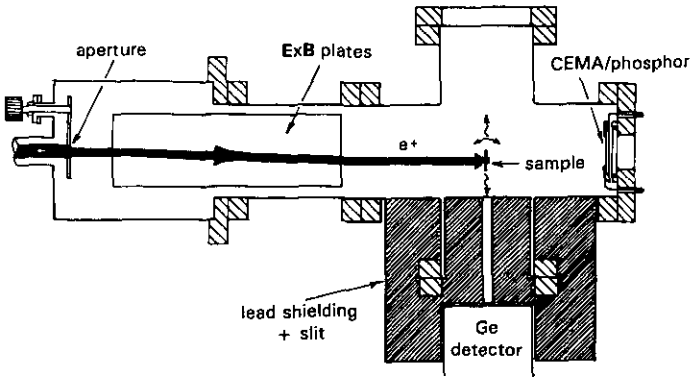

Figure 1. Schematic diagram of apparatus. Annihilation photons from the sample target pass through a 1 cm wide slit in the lead shielding surrounding the Ge detector.

The horizontal sample position x was checked by measuring annihilation count rate as the sample was moved across the slit. It was found that for each sample a plateau (i.e. constant count rate) region existed. The plateaux for all the samples overlapped, and thus a single value of x could be found which lay on each plateau and could be used for every sample.

Twenty elemental samples with atomic numbers between 4 and 82 were mounted—in sets of four or five—vertically above each other on a thin, stainless steel, electrically isolated, rotatable sample holder. Typical sample sizes were 15–25 mm square, and all were over 0.1 mm thick (i.e. effectively infinitely thick, with no positron penetration). All samples were etched and/or polished and washed prior to installation; we shall return to the effects of surface contamination later. The three magnetic samples (Cr, Fe, Ni) were mounted together and far from each other, but no measurable effect on beam position or appearance was noted. The samples were high-purity foils; no single crystals were used to reduce the influence of positron channelling. Positron beam diameters, selected by passing through an aperture approximately 1 m before the sample holder, were 8 mm for most measurements and 4 mm for the angular dependence measurements described later. In the later measurements geometrical considerations limited the maximum angle of incidence to 65°. The shape and position of the beam was monitored before each set of measurements by raising the samples and observing the beam profile with a CEMA/phosphor screen assembly at the end of the beam line. The position of the sample holder was adjusted so that the beam would hit each sample centrally by viewing the shadow of a cross at the base of the holder in the image of the beam. Each sample was then moved in turn to intersect the positron beam, with all other conditions—including the incident positron energy E—held constant.

As in [8], the positrons first pass through parallel $\boldsymbol{E} \times \boldsymbol{B}$ plates and are deflected horizontally by at least one beam diameter. This ensures that backscattered positrons are deflected again and are not able to return to the sample. Zero and negative potentials were applied to the plates so that no reflection of lower-energy backscattered positrons back to the sample could occur.

For our purposes we define backscattered positrons as those having energies greater than 50 eV; this arbitrary definition is made to avoid any ambiguity associated

with the reemission into the vacuum of any thermalized or epithermal positrons. To ensure that such positrons could not be included with those classed as having been backscattered the experiments were performed with −50 V applied to the sample holder, to prevent any slower positrons from escaping the sample. However, it was noted that annihilation count rates did not change significantly with or without the potential applied, signalling the absence of measurable slow positron emission—probably because of the conditions of the samples and their surfaces.

3. Experimental method

The incident beam intensity I_0 was deduced by measuring annihilation count rate C_{Be} for the beryllium sample. This method was preferred because no changes to the experimental configuration had to be made to perform the measurement—in contrast with, for example, the alternative method of applying a high potential to a mesh in front of the sample to prevent the escape of any backscattered positrons. A value of 3.75% was used for η_+ for beryllium at all incident energies, as suggested by Monte Carlo simulations (see later). This value is also consistent with other experimental studies. The fact that this coefficient is small and essentially energy independent leads to a small uncertainty in the estimation of I_0. Thus $I_0 = C_{Be}/0.9625$.

Annihilation count rates C were then measured for other samples mounted in the system for each energy E selected, adjusting sample positions for each new energy as described earlier. The backscattering coefficient is then evaluated from

$$\eta_+(E) = 1 - 0.9625C(E)/C_{Be}$$

with a statistical uncertainty $\Delta\eta_+$ of $\pm[C(C + C_{Be})/C_{Be}^3]^{1/2}$, i.e. typically ± 0.005 for experimental run times of 3000 s.

4. Monte Carlo simulations and transport theory

In the Monte Carlo simulations, a large number ($\sim 10^5$) of positron trajectories were followed through the target material as they interacted with the target atoms via both elastic and inelastic processes. The simulations were performed for semi-infinite Be, Al, Cu, Ag and Au. The backscattered flux was given by positrons returning to the surface with energies above 50 eV.

Elastic scattering cross-sections are obtained from a partial wave expansion [3] where the atomic scattering potential is taken from density functional calculations with the local spin density approximation. For Be, the inelastic scattering cross-sections for core electron scattering were given by the semi-empirical formula of Gryzinski [6, 12], and for valence electron scattering were determined from $\mathrm{Im}(1/\epsilon)$, where $\epsilon(q, \omega)$ is the dielectric function for momentum transfer q and energy loss ω [5]. For Be the Lindhard, i.e. free electron, dielectric function was used [3]. For inelastic scattering cross-sections for Al, Cu, Ag and Au, we have used the model dielectric function proposed by Penn [13], consisting of a weighted average of Lindhard dielectric functions for different free electron gas densities. The weighting is determined by optical data which we have taken from the *Handbook of Optical Constants of Solids* [14]. This method has the advantage of accounting for scattering

off both core and valence electrons, where the latter includes both plasmon and electron pair excitation, within a single formalism.

We have also performed a series of *electron* backscattering simulations with the elastic scattering cross sections calculated using the same model as for positrons, but with the sign of the scattering potential inverted, and with the Penn-model cross-sections describing inelastic scattering. It should be noted that the Penn model ignores the indistinguishability of the incident and target electrons (and consequently predicts electron and positron stopping powers to be nearly identical) and hence will overestimate the rate at which the electrons slow down in the solid, leading to an underestimate of the backscattering probability and of the ratio between electron and positron backscattering probabilities for reasons explained below in this section.

The simulations described here represent the most sophisticated modelling of positron transport available. However, it is instructive to consider simpler models to elucidate the origins of the dependence of η_+ with atomic number Z and incident energy E. This can be done using analytical theories like that of Vicanek and Urbassek [15]. Their theory expresses the backscattering probability for normal incidence as

$$\eta = 1 - F\left(\sqrt{t_0}\right) \tag{1}$$

where $F(x) = \exp(x^2)(1 - \mathrm{erf}(x))$ and the parameter t_0 is defined in terms of the stopping cross-section S and the transport cross section σ_{tr} as

$$t_0 = (1/3)\sigma_{tr}(E)^2 \int_0^E \left[S(E')\sigma_{tr}(E')\right]^{-1} \mathrm{d}E'. \tag{2}$$

The stopping cross-section (which is directly proportional to the stopping power) describes the effect of inelastic scattering processes while the transport cross-section accounts for the angular deflections of the particle which is primarily the result of elastic scattering. To arrive at equation (1) it is assumed that the particle initially moves ballistically on average to a depth of λ_{tr} into the solid, where λ_{tr} is the transport mean-free path calculated from σ_{tr}. The motion after this point is calculated by expanding the positron angular distribution in Legendre polynomials and neglecting higher order terms. This leads to a diffusion-like equation which can be solved analytically. Jensen *et al* [3] showed that although equation (1) does not give the correct absolute backscattering probabilities, it reproduces relative trends quite well. The equation emphasizes that the backscattering probability depends on *both* the elastic and inelastic scattering. Increased elastic scattering, i.e. higher σ_{tr}, obviously increases backscattering while increased inelastic scattering, i.e. higher stopping power, reduces the backscattering since the particle will have less time in which to suffer angular deflections which may take it back to the surface.

At high energies S and σ_{tr} can be described approximately by the Bethe–Bloch formula and the Rutherford cross-section (modified to take screening into account), respectively, which implies that the variation of S and σ_{tr} with E and Z are roughly $S \propto Z/E$ and $\sigma_{tr} \propto Z^2/E^2$. Hence, from equations (1) and (2) above, within this approximation, t_0 and thus η are independent of E. Similarly, t_0 varies linearly with Z which implies that η varies approximately as $Z^{1/2}$ since $1-F(x) \simeq x$ for small x. Thus the model predicts an increase of η with Z due to the fact that the elastic scattering increases faster with Z than the inelastic scattering, while the energy

dependences of elastic and inelastic scattering tend to cancel each other out at high energies leading to approximately energy-independent values of η.

It is possible to make a rough estimate for the effects of indistinguishability using this transport model and the stopping powers calculated for electrons and positrons by Ashley [16] who did allow for the indistinguishability in the case of electrons. Ashley's results [16] indicate that for incident energies of between 5 and 50 keV, the ratio between electron and positron stopping powers is approximately 0.8 and this ratio depends only weakly on the incident energy and the material. Hence, the true value of t_0 for electrons is expected to be about 20% higher than the values that would be obtained from the Penn model. From equation (1), η is approximately proportional to $t_0^{1/2}$, so that using the Penn model for electrons leads to an underestimate of η_- by about 10%. This suggests that our simulated values for η_- and thus the ratio η_-/η_+ should be corrected by a factor of 1.1 to allow for the indistinguishability effect.

5. Results

Figures 2 and 3 show experimental and simulations results for $\eta_+(Z)$ at 5 and 30 keV respectively together with the earlier results of Baker and Coleman [8], the integrated results of Massoumi *et al* [10], and the very recent results of Mäkinen *et al* [21]. The last researchers used the technique of Baker and Coleman [8]. Also shown for comparison are the electron coefficients $\eta_-(Z)$ of Bishop [17] at 5 keV and of Neubert and Rogaschewski [18] at 30 keV.

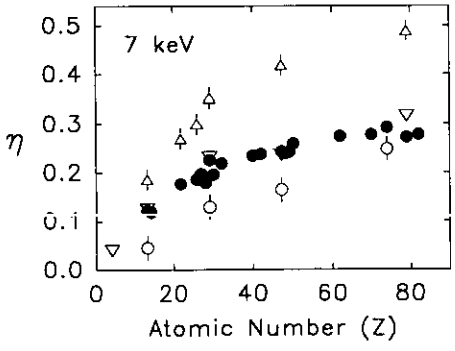

Figure 2. Total backscattering coefficients versus atomic number for 7 keV positrons. ●, current data. Statistical error bars lie within the points. ▽, Monte Carlo simulations (at Z = 4, 13, 29, 47 and 79). ○, results of Baker and Coleman [8]. △, electron coefficients for E = 5 keV [17].

Figure 4 gives experimental and simulated values for η_+ for Be, Al, Cu, Zn and Au for energies E of 1, 3, 7 and 30 keV.

Figure 5 shows measurements and simulations for $\eta_+(E)$ for Be, Al, Cu, Zn and Au for energies E between 1 and 50 keV, together with composite results for $\eta_-(E)$ obtained by Bishop [17], Neubert and Rogaschewski [18] and Fitting [19].

Figure 6 illustrates the dependence of measured and simulated coefficients on angle of incidence θ for Al and Au at 5 and 35 keV. Data for 40 keV electrons

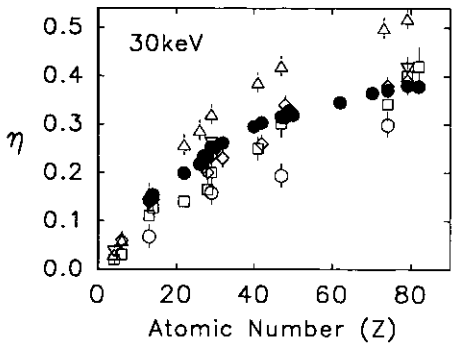

Figure 3. Total backscattering coefficients versus atomic number for 30 keV positrons. ●, current data. ▽, Monte Carlo simulations (at Z = 4, 13, 29, 47 and 79). ○, results of Baker and Coleman [8]. □, results of Massoumi *et al* for E = 35 keV [10]. ◇, results of Mäkinen *et al* [21]. △, electron coefficients of Neubert and Rogaschewski [18].

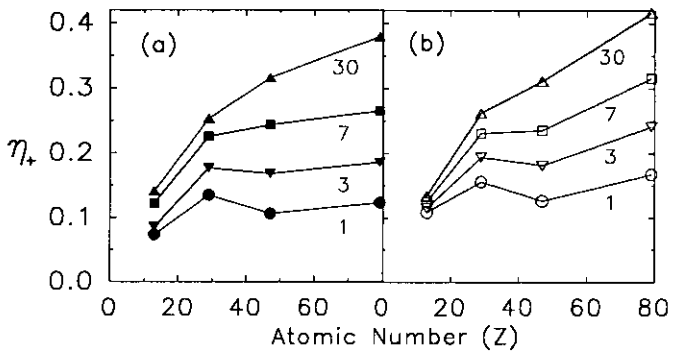

Figure 4. Positron backscattering coefficients versus atomic number for incident energies 1 keV (●, ○), 3 keV (▼, ▽), 7 keV (■, □) and 30 keV (▲, △): (*a*) experimental and (*b*) Monte Carlo results. Lines joining points are to aid the eye only.

from [18] are included; the difference between 35 and 40 keV results for electrons is expected to be unimportant and so comparison with the positron data is valid.

The full set of experimental and simulated data for η_+ is given in tables 1 and 2.

Figure 7 shows how the ratio η_-/η_+ varies with Z, with η_- taken from experimental data from [17–19]. (Because the technique used to measure η_+ by the authors is not applicable to electron measurements, results for electrons have been taken from other laboratories.) Figure 7 also shows predictions from Monte Carlo simulation together with a corrected set of predictions that take into account the effects of indistinguishability described in section 4.

Figure 8 shows the energy dependence of η_-/η_+ obtained from experiment, together with corrected Monte Carlo results.

6. Discussion

The results shown in figures 2 and 3 suggest a smooth, monotonically-increasing dependence of η_+on atomic number Z. There is excellent agreement between

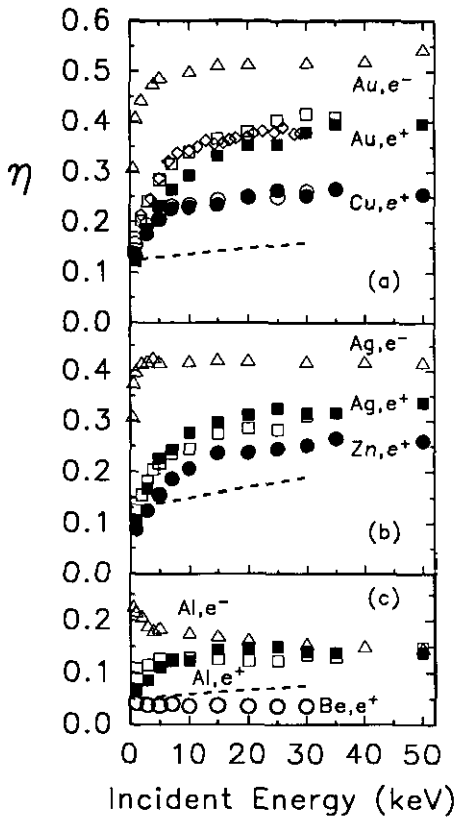

Figure 5. Total backscattering coefficients versus incident positron energy. (*a*) ●and ○, current experimental and Monte Carlo results for copper. ■and □, the same, for gold. ◊, recent results of Mäkinen *et al* [21]. △, composite electron results for gold from [17–19]. ----, representation of results for copper of Baker and Coleman [8]. (*b*) ●, experimental results for zinc. ■and □, experimental and Monte Carlo results for silver. △, composite electron results for silver from [17–19]. ----, representation of results for silver of Baker and Coleman [8]. (*c*) ○, Monte Carlo results for beryllium. ■and □, experimental and Monte Carlo results for aluminium. △, composite electron results from [17–19]. ----, representation of results for aluminium of Baker and Coleman [8].

experiment and Monte Carlo simulations, and closer agreement of both with other recent measurements than with the earlier results of Baker and Coleman [8]. It is evident that the data at E = 30 keV (figure 3) are smoother than those for E = 7 keV (figure 2). The reason for this presumably lies in the sensitivity of the measurements at lower energies (i.e. < 10 keV) to surface contamination. After removal from the vacuum system for further surface cleaning, and/or ion sputtering *in situ*, η_+ values measured below 10 keV were found to increase for a number of samples including Cu, Ge, Sn, Ag, Pb and Au, the change being greatest at the lowest incident energies; e.g. η_+ at E = 3 keV rose from 0.095 to 0.162 for Ag after recleaning. Other samples—e.g. Al—showed little or no change after cleaning. This sensitivity to contamination is attributed to backscattering coefficients associated with adsorbate species being in general lower than the bulk atoms under study. As a consequence of these considerations it is suggested that the 'true' locus of $\eta_+(Z)$

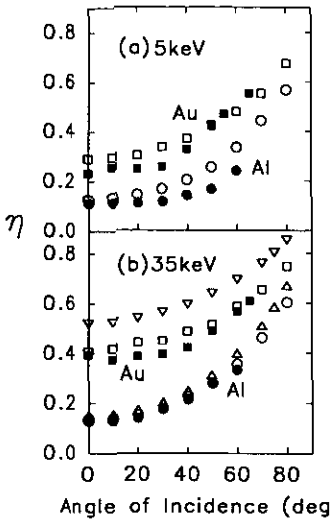

Figure 6. Total positron backscattering coefficients versus angle of incidence. (*a*) Incident positron energy 5 keV: ●and ○, experimental and Monte Carlo results for aluminium; ■and □, the same for gold. (*b*) Incident positron energy 35 keV; symbols as in (*a*). △and ▽, electron results for aluminium and gold (E = 40 keV) from [18].

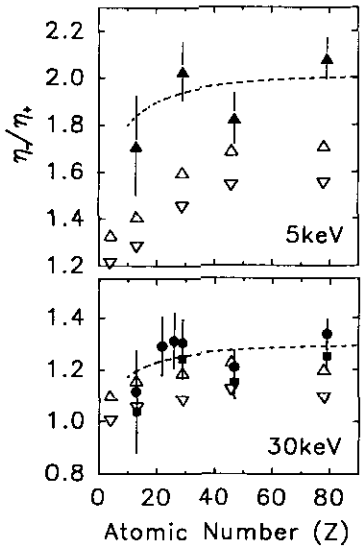

Figure 7. Ratio of electron to positron backscattering coefficients versus Z. ●, η_- from [10] for 35 keV electrons, η_+ from current experimental results for 30 keV positrons. ■, the same, but using η_- from [17]. ▲, η_- from [17] for 5 keV electrons, η_+ from current results for 7 keV positrons. Broken lines are fits to aid the eye. ▽, Monte Carlo results; △, corrected Monte Carlo results (1.1 x uncorrected—see text).

Table 1. Experimental (expt) and simulation (MC) results for total backscattering coefficients (%). Uncertainties in the last significant digits are shown in parentheses.

Z \ E(keV)		1	3	5	7	10	15	20	25	30	35	50
4	MC	4.2(2)	3.8(2)	3.7(2)	4.0(2)	3.6(2)	3.7(2)	3.5(2)	3.6(2)	3.6(2)		
13	expt	6.9(8)	8.6(8)	11.2(9)	12.2(8)	12.3(8)	14.4(8)	14.6(8)	15.0(8)	14.1(8)	13.8(5)	13.9(5)
	MC	10.9(3)	11.5(3)	12.6(4)	12.5(4)	12.8(4)	12.6(4)	12.3(4)	12.3(4)	13.4(4)	13.0(1)	14.7(4)
14	expt				11.8(8)					15.3(7)		
22	expt				17.7(7)					19.9(7)		
26	expt				18.6(7)					21.8(8)		
27	expt				19.7(7)					23.3(8)		
28	expt				17.9(7)					23.2(8)		
29	expt	13.5(5)	17.7(5)	20.5(5)	22.6(5)	22.9(5)	23.4(5)	25.2(5)	26.5(5)	25.3(5)	26.6(5)	25.5(5)
	MC	15.6(4)	19.4(4)	20.5(5)	23.1(5)	23.5(5)	24.4(5)	25.0(5)	25.0(5)	26.2(5)	--	--
30	expt	8.9(5)	12.5(5)	15.6(5)	18.6(5)	20.6(5)	23.7(5)	23.8(5)	24.6(5)	25.3(5)	26.6(5)	26.1(5)
32	expt				21.9(8)					26.2(7)		
40	expt				23.4(8)					29.5(6)		
42	expt				23.8(7)					30.4(6)		
47	expt	10.6(8)	16.8(8)	22.7(8)	24.3(8)	27.7(8)	29.8(8)	31.3(8)	32.6(8)	31.6(6)	31.7(5)	33.7(5)
	MC	12.6(4)	18.2(4)	21.6(5)	23.6(8)	24.5(5)	27.5(5)	28.6(5)	28.3(5)	31.1(6)	--	--
48	expt				23.9(7)					31.5(6)		
49	expt				24.2(7)					32.8(6)		
50	expt				25.9(8)					32.0(6)		
62	expt				27.5(7)					34.6(7)		
70	expt				27.8(7)					36.5(6)		
74	expt				29.3(7)					37.1(6)		
79	expt	12.3(5)	18.6(5)	23.2(5)	27.3(5)	29.4(5)	33.2(5)	35.4(5)	35.6(5)	38.0(5)	39.5(5)	39.6(5)
	MC	16.8(4)	24.2(5)	29.02	31.6(6)	34.0(6)	36.6(6)	38.1(6)	40.4(6)	41.6(6)	40.9(2)	--
82	expt				27.8(8)					37.9(6)		

Table 2. Total positron backscattering coefficients versus angle of incidence for Al and Au. Convention is as for table 1.

	θ(deg.)	0	10	20	30	40	50	55	60	65	70	80
Al	expt	11.2(9)	11.3(9)	11.0(9)	11.6(9)	14.1(9)	16.6(9)	--	24.0(9)	--	--	--
5keV	MC	12.6(4)	13.4(4)	14.3(4)	16.7(4)	20.3(5)	25.4(5)		33.4(6)		44.3(7)	56.8(8)
Al	expt	13.8(5)	13.7(7)	14.1(7)	17.7(7)	21.5(7)	27.8(7)	--	33.3(6)	--	--	--
35keV	MC	13.0(1)	13.2(4)	15.2(4)	17.9(1)	22.0(2)	27.9(3)		35.5(2)		46.1(3)	60.2(3)
Au	expt	23.2(5)	25.6(8)	24.7(8)	25.6(8)	32.6(6)	42.6(7)	46.8(7)	--	55.3(6)	--	--
5keV	MC	29.0(5)	29.5(5)	30.1(5)	33.6(6)	36.9(6)	42.2(6)	--	47.8(7)	--	55.2(7)	67.3(8)
Au	expt	39.5(5)	37.7(6)	38.5(6)	39.5(6)	42.1(6)	48.9(5)	--	56.6(5)	60.9(5)	--	--
35keV	MC	40.9(2)	41.9(6)	44.1(7)	44.9(2)	48.6(5)	51.3(5)		58.7(2)		65.5(6)	74.8(4)

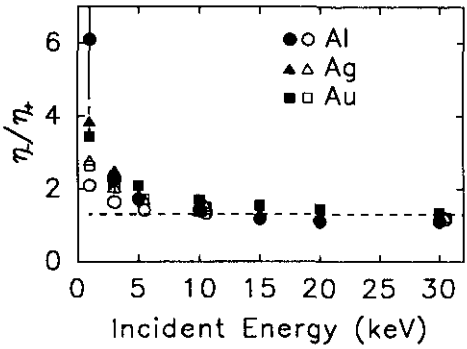

Figure 8. Ratios of electron to positron backscattering coefficients versus incident particle energy for aluminium (●), silver (▲), and gold (■). η_+ are current experimental values; η_- are composite results from [17–19]. Open symbols are corrected (× 1.1) Monte Carlo results (see text).

at 7 keV (figure 2) should be drawn through the higher experimental values, rather than as a best fit to all of the data points. The earlier results of Baker and Coleman [8] do appear to be considerably lower than the new measurements; the nature of the discrepancy appears to be consistent with a lack of discrimination against the detection of a fraction of the backscattered positrons in the earlier experiments, which becomes more severe as the incident energy E increases.

The fact that both $\eta_+(Z)$ and $\eta_-(Z)$ vary approximately as $Z^{1/2}$ at high energies is consistent with the predictions of the transport model described in section 4 above, where a physical explanation for this behaviour is given. However, figure 4 clearly shows that $\eta_+(Z)$ at low energies is not a monotonic function of Z. This indicates that there are deviations in the cross-sections from the simple high-energy behaviour described in section 4.

The agreement between Monte Carlo simulations and experiment for the $\eta_+(E)$ and $\eta_+(\theta)$ results shown in figures 5 and 6 is gratifying, although the discrepancy in $\eta_+(E)$ for Al at low energies may well be explained by the persistence of surface contamination effects. These may also be the reason why the measured $\eta_+(\theta)$ for Al does not rise as steeply as the simulation predicts (surface contamination becomes more important as grazing incidence is approached and the mean implantation depth decreases).

Howell *et al* [20] demonstrated that backscattering positrons can pick up electrons on leaving a surface. Para-positronium (p-Ps) thus would decay before leaving the detector window in the current experiment, and detection of its decay gamma rays

would lead to an underestimation of η_+. However, Howell *et al* showed that the probability of electron pickup by fast positrons is significant only at energies below about 1 keV; furthermore, p-Ps constitutes only 25% of the total Ps formed (the longer-lived ortho-Ps decays out of sight of the detector). We therefore estimate that for incident positron energies between 1 and 50 keV the effect on η_+ of the detection of p-Ps gamma radiation will be of the order of 1% or less.

The results predicted in figures 7 and 8 confirm the conclusion of Massoumi *et al* [10] that a constant value of 1.3 for $\eta_-/\eta_+(Z)$ is reasonable at high incident energies E. We show that this ratio rises significantly at low E—e.g. closer to 2 at 5 keV—and may show a slight positive slope with Z. Figure 7 shows clearly that the Penn Monte Carlo predictions all lie below the experimental data. This can be explained by the fact mentioned in section 4 that the cross-sections used for inelastic scattering by conduction electrons based on the Penn model ignore the indistinguishability of the incident and target electrons. Hence, the rate at which electrons slow down in the solid is underestimated, leading to an underestimate of the backscattering probability. Note that this is the case despite the fact that we have used elastic scattering cross-sections that are appropriate for electrons. We can obtain an improved, though not perfect, agreement with the experimental data by making the correction of 10% discussed at the end of section 4. This suggests that we can reproduce the experimental data quite well once indistinguishability is taken into account. The better agreement at higher energies may indicate the unavoidable corruption of the electron data at lower incident energies by the inclusion of high-energy secondary electrons in the backscattered flux, which would lead to an overestimation of η_-.

7. Conclusions

New measurements and Monte Carlo simulations of total backscattering coefficients η_+ versus Z, E and θ show pleasing agreement with each other and with each other recent measurements. This agreement further strengthens the validity of the Monte Carlo code of Jensen and Walker, full details of which are to be published, which can therefore be used with confidence to deduce positron implantation profiles and related positron parameters which are fundamental to a wide array of developing investigative techniques using positrons. The qualitative behaviour of electron and positron backscattering coefficients with E and Z agrees with predictions of the analytical transport model of Vicanek and Urbassek [15] which has also been used to shed light on the roles of the elastic and inelastic scattering processes. Modification of the Monte Carlo code to describe electron implantation should prove valuable in numerous applications.

Acknowledgments

KOJ and LA would like to thank the SERC and DAAD (Germany), respectively, for support.

References

[1] Schultz P J and Lynn K G 1988 *Rev. Mod. Phys.* **60** 701

[2] Massoumi G R, Hozhabri N, Jensen K O, Lennard W N, Lorenzo M S, Schultz P J and Walker A B 1992 *Phys. Rev. Lett.* **68** 3873
[3] Jensen K O, Walker A B and Bouarissa N 1990 *Positron Beams for Solids and Surfaces* ed P J Schultz, G R Massoumi and P J Simpson (New York: AIP) p 19
[4] Jensen K O and Walker A B 1992 *Surf. Sci.* submitted
[5] Baker J A, Chilton N B, Jensen K O, Walker A B and Coleman P G 1991 *J. Phys.: Condens. Matter* **3** 4109; *Appl. Phys. Lett.* **59** 2962
[6] Valkealahti S and Nieminen R M 1984 *Appl. Phys.* A **35** 51
[7] Mills Jr A P and Wilson R J 1982 *Phys. Rev.* A **26** 490
[8] Baker J A and Coleman P G 1988 *J. Phys. C: Solid State Phys.* **21** L875
[9] Coleman P G and Baker J A 1989 *Acta Univ. Wratislaviensis* No 1204, p 37
[10] Massoumi G R, Hozhabri N, Lennard W N and Schultz P J 1991 *Phys. Rev.* B **44** 3486
[11] Hutchins S M, Coleman P G and West R N 1985 *Positron Annihilation* ed P Jain, R M Singru and K P Gopinathan (Singapore: World Scientific) p 983
[12] Gryzinski M 1965 *Phys. Rev.* A **138** 322
[13] Penn D R 1987 *Phys. Rev.* B **35** 482
[14] Palik D 1985 *Handbook of Optical Constants of Solids* (Orlando, FL: Academic)
[15] Vicanek M and Urbassek H M 1991 *Phys. Rev.* B **44** 7234
[16] Ashley J C 1990 *J. Electron Spectrosc. Relat. Phenom.* **50** 323
[17] Bishop H E 1967 *Br. J. Appl. Phys.* **18** 703
[18] Neubert G and Rogaschewski S 1980 *Phys. Status Solidi* a **59** 35
[19] Fitting H J 1974 *Phys. Status Solidi* a **26** 525
[20] Howell R H, Rosenberg I J and Fluss M J 1986 *Phys. Rev.* B **34** 3069
[21] Mäkinen J, Palko S, Martikainen J and Hautojärvi P 1992 *J. Phys.: Condens. Matter* **4** 503